

pubs.acs.org/crystal Article

Half-Heusler Structures with Full-Heusler Counterparts: Machine-Learning Predictions and Experimental Validation

Alexander S. Gzyl, Anton O. Oliynyk, and Arthur Mar*



Cite This: *Cryst. Growth Des.* 2020, 20, 6469–6477

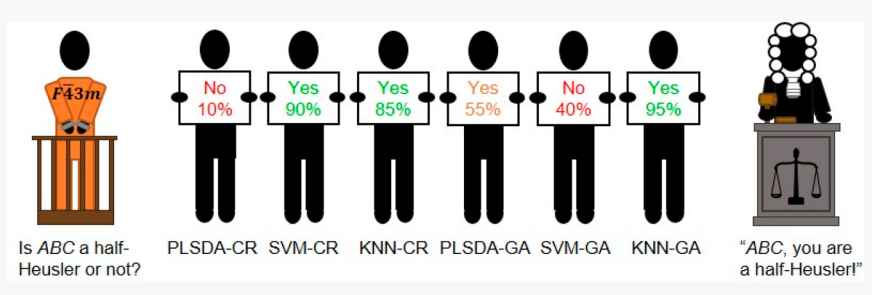


ACCESS

Metrics & More



s Supporting Information



ABSTRACT: Heusler compounds form a diverse group of intermetallic materials encompassing many compositions and structures derived from cubic prototypes, and exhibiting complicated types of disorder phenomena. In particular, preparing solid solutions between half-Heusler ABC and full-Heusler compounds AB₂C offers a means to control physical properties. However, as is typical in materials discovery, they represent only a small fraction of possible intermetallic compounds. To address this problem of unbalanced data sets, a machine-learning model was developed using an ensemble approach involving the synthetic minority oversampling technique to predict new compounds likely to adopt half-Heusler structures. The training set was based on experimental crystal structures, including those of nonstoichiometric compounds. The model achieved an accuracy of 98% on the validation set and gave excellent performance in terms of balanced statistical measures. A subset of compounds predicted to adopt half-Heusler structures having existing full-Heusler counterparts was then targeted for preparation. Six of seven of these candidates were successfully synthesized and confirmed to be half-Heusler compounds.

INTRODUCTION

The large family of ternary and quaternary intermetallic compounds collectively known as Heusler compounds are important for many applications, 1,2 including thermoelectric materials,^{3–5} ferromagnets,^{6,7} magnetocaloric materials,⁸ topological insulators and superconductors, 9,10 shape memory alloys, 11 and, most recently, catalysts. 12 The remarkable versatility can be traced to the compositional and structural richness of these compounds, which span at least four cubic structure types termed (full)-Heusler (Cu₂MnAl-type), ¹³ half-Heusler (MgAgAs-type), inverse Heusler (Li2AgSb-type, sometimes also called Hg₂CuTi-type), and quaternary Heusler (LiMgPdSn-type). Half-Heusler structures are adopted by ternary compounds with a composition of 1:1:1, full and inverse Heusler structures are adopted by ternary compounds with a composition of 2:1:1 (or 1:2:1, depending on the sequence of elements written in a formula), and quaternary Heusler structures are adopted by quaternary compounds with a composition of 1:1:1:1. Compounds having a tetragonal Heusler (VRh₂Sn-type) structure can also result from the distortion of the cubic prototypes, and they are of interest for spintronic applications. 14,15 If all metallic elements are considered, the possible combinations of elements are so numerous (>10⁵ for ternary and >10⁶ for quaternary

compounds) that exploratory synthesis to discover new intermetallic compounds is a herculean task. Empirical observation suggests that not all combinations are permitted. Restricting to combinations of an early d-block metal, a late dblock metal, and a p-block metal or metalloid, which constitute most known ternary Heusler compounds, reduces the number of possibilities, but the frequent occurrence of site disorder and vacancy defects complicates matters. Currently, Pearson's Crystal Data reports 1371 ternary Heusler compounds (Cu₂MnAl-, MgAgAs-, and Li₂AgSb-type), of which 637 (46%) have undergone structure determination and 78 (5%) have been analyzed by single-crystal X-ray diffraction (XRD).¹⁶ Most of the structural characterization has been limited to powder X-ray diffraction, which can be inconclusive when the intensities of diagnostic peaks are very weak or nearly indistinguishable for different structural models. Discovering

Received: May 10, 2020 Revised: August 31, 2020 Published: September 1, 2020





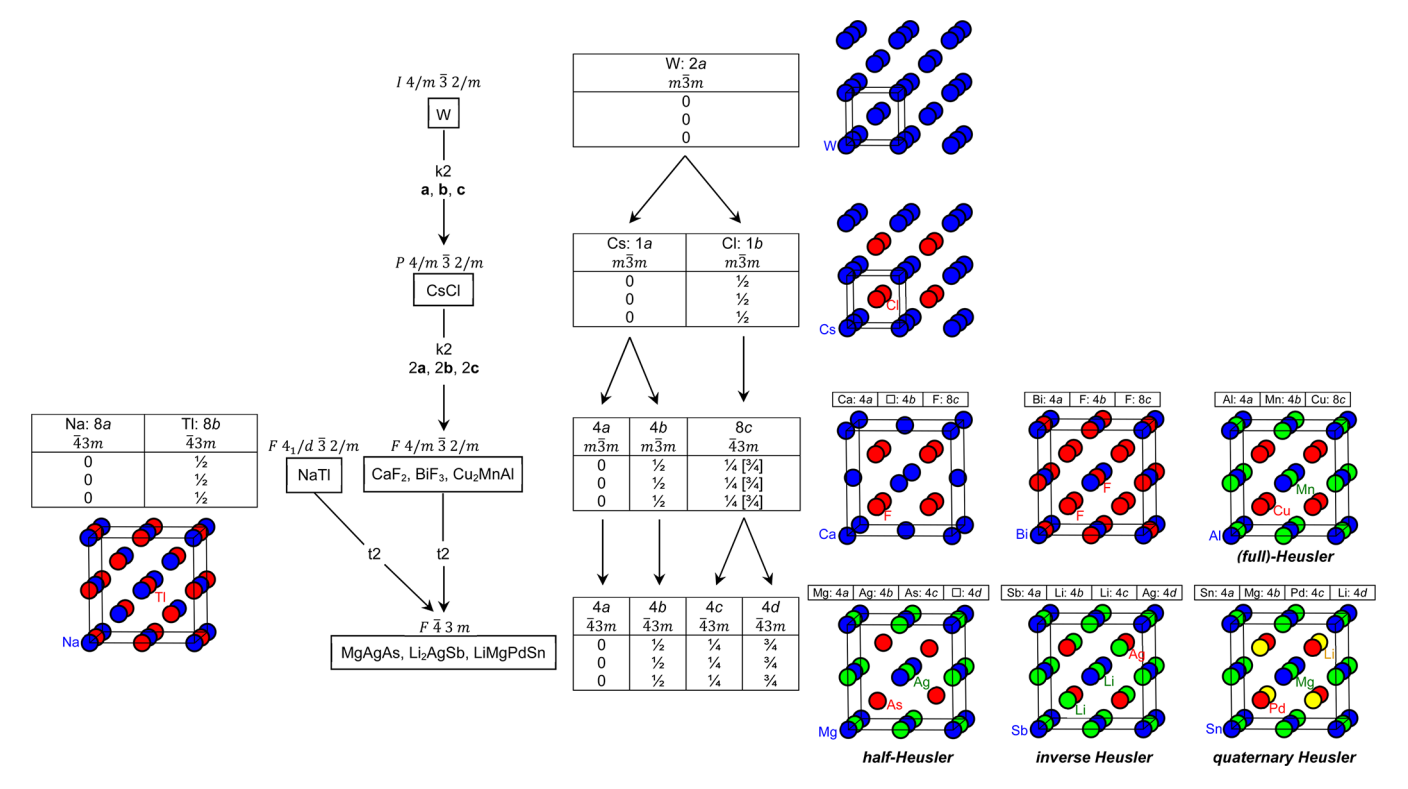


Figure 1. Bärnighausen tree showing group-subgroup relationships of structures adopted by Heusler compounds, including those that exhibit disorder.

new Heusler compounds or characterizing existing ones would thus benefit from additional guidance.

The structures presented above represent idealizations: Heusler compounds actually exhibit many types of disorder phenomena, expanding the compositional possibilities even further (e.g., by introducing deviations from the ideal 1:1:1, 1:2:1, or 1:1:1:1 compositions). The most frequent type is substitutional disorder, which occurs when a site is occupied by more than one type of atom. For ternary Heusler compounds, these possibilities have been enumerated, 17 but experimental confirmation lags far behind, because the chemical space to explore is so huge. Although disorder could be viewed as a nuisance, it offers a powerful tool to control physical properties, because small amounts of disorder can have profound effects on the electronic structure and on the performance of magnetic, magnetocaloric, or thermoelectric materials. For example, substituting Ti for Nb in Ti, Nb_{1-x}CoSn causes transitions from a nonmagnetic semiconductor to a ferromagnetic metal, 18 and self-doping with Ni in ZrNiSn improves thermoelectric properties by reducing thermal conductivity by over 60%. 19 Another type of disorder, though less commonly reported, arises from vacancy defects. For example, as vacancies are gradually introduced in MnNi_{2-x}Sb (x = 0-1), the structure transforms from full- to half-Heusler, and the magnetocaloric response is modified.^{20,21} This transformation could also be described in the reverse way as the occupation of interstitial sites on progressing from the half- to full-Heusler structure in MnNi_{1+x}Sb (x = 0-1). An exciting recent development is the application of this disorder phenomenon to improve the performance of thermoelectric devices by "nanostructuring," in which interfaces are constructed between full- and half-Heusler structures. 22-26

A Bärnighausen tree²⁷ illustrates the group-subgroup relationships between the most common structure types

adopted by Heusler compounds, including those that are disordered; essentially, they are all superstructures of bodycentered cubic (bcc) packing (Figure 1). Within any one of these structures, disorder arises when a given set of crystallographic sites (identified by a Wyckoff letter) accommodates a mixture of two or more atoms (or vacancies). For example, the W-type structure represents the extreme situation of complete disorder, when all elemental components are randomly distributed in the sites, with no preference. Upon close examination of the relationships illustrated here, the transformation from half- to full-Heusler structures can be realized through multiple pathways. As additional atoms are introduced into the half-Heusler structure (space group $F\overline{4}3m$), they could preferentially enter the vacant 4d sites exclusively, thus preserving the space group symmetry, or both the 4c and 4d sites could be partially occupied equally, thus merging into the symmetry-equivalent Wyckoff set 8c found in the full-Heusler structure (space group $Fm\overline{3}m$). The more general problem is understanding how any of the structures that could be adopted by compounds with a composition of 1:1:1 (e.g., MgAgAs-, CaF2-type) transform on the path to those structures adopted by compounds with a composition of 2:1:1 (e.g., Cu₂MnAl-, Li₂AgSb-, LiMgPdSn-type).

Several approaches have been applied to rationalize the formation of Heusler compounds and to predict their structures and properties. Through empirical observations, various rules have been formulated based on simple concepts such as electron counting and electronegativity differences. However, these rules are fallible, with exceptions being treated by devising new rules pertaining to special situations (such as preferred site occupation by specific elements). First-principles calculations generally proceed by comparing total energies to assess the stability of competing phases. 15,28–32 When implemented with high-throughput methods, large numbers

of models can be analyzed very rapidly. 25,33-38 However, as Legrain et al. have shown, inconsistent results can be obtained by separate practitioners to predict new half-Heusler compounds, suggesting that other factors (such as configurational entropies) are important to consider.³⁹ Further, although computational predictions should ideally be tested through experimental validation, it is disconcerting that this is rarely carried out; worse, when such predictions are proven wrong, they are forgotten. 40 As an alternative approach, machine-learning models based on training through empirical data have been developed to predict new Heusler compounds and their site preferences. 39,41,42 The success of these machinelearning models depends on the availability of abundant and reliable experimental data. Regardless of the specific approach, most of these studies have tended to focus on Heusler compounds with ordered structures being assumed. Treatment of disorder by first-principles methods remains a challenging problem.

As part of a broad effort to apply machine-learning methods to discover new intermetallic compounds, 43 including Heusler compounds, we present here an investigation motivated by several aims. First, within the context of method development, we wish to evaluate how combining an ensemble approach with the synthetic minority oversampling technique (SMOTE)⁴⁴ can help address the problems of unbalanced data sets and overfitting, which are typical when applying machine-learning methods in materials discovery. 45,46 This ensemble approach is applied to the problem of predicting new half-Heusler compounds, and its performance is compared with that of a random-forest model previously developed by Legrain et al.³⁹ Second, among the candidates predicted to adopt half-Heusler structures, a subset of these are sought that are likely to exhibit a continuous solid solution between halfand full-Heusler structures. In other words, this aim could be rephrased as the question, "Can a hypothetical half-Heusler compound ABC be identified that also has an existing full-Heusler compound counterpart AB₂C consisting of the same three elements?" Third, we attempt to synthesize some of these predicted compounds and characterize them with X-ray diffraction.

■ EXPERIMENTAL SECTION

Machine-Learning Pipeline. A model to predict the occurrence of half-Heusler structures ABC was developed by applying machinelearning algorithms to detect patterns in a training set of crystallographic data on the basis of chemical descriptors. The data consisted of all entries found within the latest release of Pearson's Crystal Data¹⁶ that have the chemical formula ABC, including those deviating from the ideal equiatomic composition by up to 20%, that contain elements up to Bi (Z = 83), as well as U or Th, but not hydrogen or noble gases. In total, there were 2818 such compounds, of which 180 adopt the MgAgAs-type structure. Descriptors were derived from 55 atomic properties of each element (Table S1 in the Supporting Information); these properties were then combined through 21 types of arithmetic operations (Table S2 in the Supporting Information), giving a total of 1155 descriptors to be considered at the outset of building the machine-learning model. The machinelearning pipeline was built using the PLS_Toolbox software (version 8.0.1)⁴⁷ within the MATLAB (2018a release) environment.⁴⁸ Twothirds of the data were assigned to a training set, and one-third was assigned to a validation set. The data were preprocessed by autoscaling (mean-centering of columns and dividing by standard deviations to obtain unit variance) and normalization (dividing by sum of absolute values of each row).

The prediction probabilities obtained from three different algorithms available in PLS_Toolbox (k-nearest neighbors (KNN), support vector machine (SVM), and partial least-squares discriminant analysis (PLS-DA)) were combined by soft-voting, using scripts written in MATLAB. Two types of procedures to select descriptors (cluster-resolution feature selection (CR-FS) and genetic algorithm (GA)) 49,50 were used to generate six models in total (Figure 2a). In

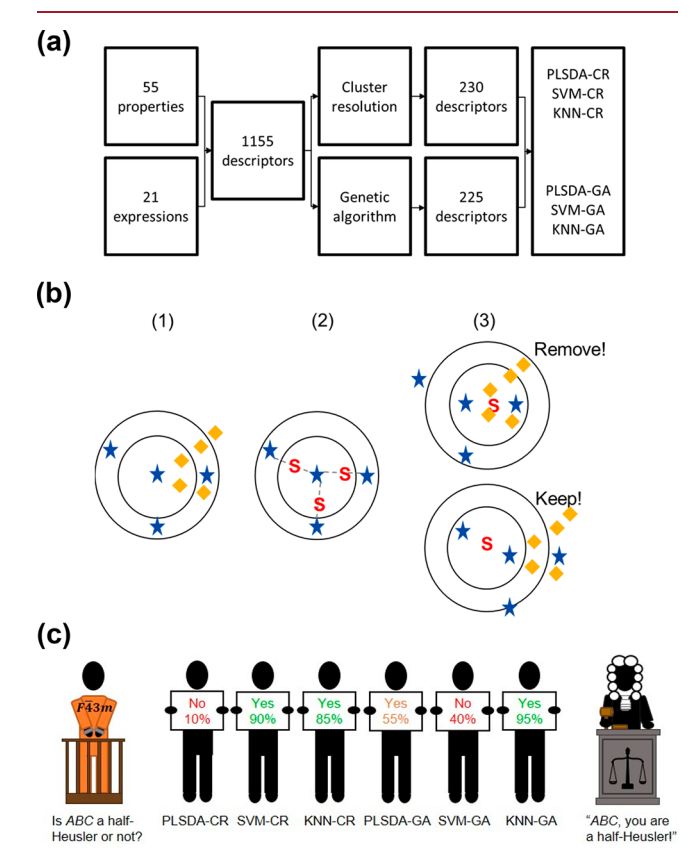


Figure 2. (a) Machine-learning workflow: Combining 55 atomic properties through 21 mathematical expressions generated 1155 descriptors, of which subsets were selected through a cluster-resolution feature selection or genetic algorithm to be used in conjunction with three types of algorithms. (b) SMOTE technique: Within an unbalanced data set containing minority (\bigstar) and majority (\bigstar) samples, synthetic samples (S) are generated between pairs of minority samples. Synthetic samples are kept if most of the nearest neighbors are also minority samples but removed if not. (c) Example of soft-voting procedure among an ensemble of models: The probabilities of a given candidate ABC to be a half-Heusler compound as evaluated by different machine-learning models are averaged to arrive at a decision about the classification.

CR-FS, the features were selected by initially ranking them according to their Fisher ratio scores and then retaining those in a backward elimination step and adding those in a forward selection step by evaluating how a feature affects model quality based on a metric called cluster resolution. 49 Three iterations with 100 rounds of CR-FS were performed, giving 300 sets of descriptors; among these sets, the one that performed best in terms of validation accuracy contained 230 descriptors having the highest survival rate. One iteration of GA was run, using a population size of 256, which corresponds to the largest population setting to increase the number of possibilities to perform crossover and to improve accuracy. The maximum number of generations was set to 200, sufficient for the algorithm to converge on a solution. The mutation rate was set to 0.005 to address under- or overrepresentation of descriptors in the populations, with double crossover used as the breeding strategy. Partial least-squares was used as the regression method to evaluate chromosomes in the population,

with 25 latent variables and 10-fold-split random cross validation. The fittest model contained 225 descriptors. Algorithms in PLS_Toolbox were optimized according to their analysis flowcharts. The KNN algorithms used an optimal k-value determined iteratively to be 4, based on cross-validation accuracy. The SVM algorithms used a Gaussian radial basis function as the kernel. The PLS-DA algorithms gave the best performance using 20 latent space variables.

Because the number of known half-Heusler compounds constitutes only a small fraction of the much larger set of ABC compounds, the data set is highly imbalanced and biased against the minority class (half-Heusler compounds) in this classification problem. To correct this imbalance, the data set was augmented through SMOTE, ⁴⁴ which acts to improve the representation of samples in the minority class (Figure 2b).

First, the *k*-nearest neighbors around a given sample in the minority class are identified. A k-value of n-1, where n is the number of samples in the minority class, was selected to generate the maximum number of neighbors for each sample. Then, between each neighbor, a synthetic sample is placed, which is intended to be as similar as possible to the minority samples. These synthetic samples are added to the data set. The KNN procedure is performed again on the whole data set to find the nearest neighbors of each synthetic sample. If 60% of the nearest neighbors of the synthetic samples belong to the minority class, they are kept in the data set; otherwise, they are discarded. Starting from a value of 3, k was adjusted to ascertain how it affects the number of synthetic samples generated. The k-value that resulted in the largest number of synthetic samples was accepted for each feature set (k = 10 for GA and k = 11 for CR-FS). Within the training set, a total of 52 synthetic samples were generated for the models using GA, and 625 were generated for the models using CR-FS. The models were then considered together as an ensemble (Figure 2c). The votes from each model were combined through soft voting, which examines the average of the prediction probabilities; if the average probability exceeds 50%, then a given sample is labeled as half-Heusler. The best combination of SMOTE models was then selected based on the performance measures (sensitivity, specificity, and accuracy), resulting in an ensemble consisting of five models (with PLSDA-CR being excluded).

Synthesis and Characterization. Reactions were performed in attempts to prepare some of the top-ranked candidates ABC to adopt half-Heusler structures as predicted from the machine-learning model, in particular, those that also have an existing counterpart AB2C having a full-Heusler structure and composed of the same set of elements. The following details pertain to the attempted preparation of MnRhPb, MnPdSn, MnRhSn, MnPdIn, MnNiSn, MnRuSb, and VRhSn. The starting materials were Mn powder (99.95%, Alfa-Aesar), fresh filings from V rod (99.5%, Alfa-Aesar), Ru sponge (99.95%, Alfa), Rh powder (99.95%, Alfa), Ni powder (99.9%, Cerac), Pd powder (99.95%, Alfa), In powder (99.9%, Alfa), Sn powder (99.8%, Cerac), Pb powder (>99%, Sargent), and Sb powder (99.6%, Fisher). The elements were combined in equimolar ratios with a total mass of 0.3 g, and, where necessary, an excess of any of the more volatile components (e.g., Mn, Sb, Pb) was added. The mixtures were pressed into pellets, which were arc-melted three times (the pellets being flipped each time) under an argon atmosphere in an Edmund Bühler MAM-1 arc melter. The arc-melted ingots were placed in fused-silica tubes, which were evacuated, sealed, and heated at 800 °C for three weeks followed by quenching in cold water. Synthesis through direct reactions, without arc-melting, was also attempted by heating equimolar mixtures of the elements, pressed into pellets, at 800 °C (VRhSn, MnNiSn, MnRuSb) or 1000 °C (VRhSn, MnRuSb, MnPdIn, MnRhSn) for one week, followed by cooling to room temperature over 48 h.

Reactions were also performed to target candidates with low probabilities (<50%) of adopting half-Heusler structures: CrGaSn, CrMoNi, CuRuNb, MoHfNi, NiAgNb, VHfAg, and ZrRuNb. These candidates were chosen such that at least one of the elemental components is shared in common with the compositions of the high-probability counterparts above. The starting materials were Zr sponge (99.5%, Alfa), Hf powder (>99%, Onyx), fresh filings from V rod

(99.5%, Alfa-Aesar), Nb powder (>99%, Onyx), Cr powder (99%, Alfa-Aesar), Mo powder (>99%, Mackay), Ru powder (>99%, Onyx), Ni powder (99.9%, Cerac), Cu powder (99%, Alfa), Ag powder (>99%, Alfa), Ga ingot (99.99%, Cerac), and Sn powder (99.8%, Cerac). Equimolar mixtures of the elements were subjected to three types of treatments: (i) arc-melting; (ii) heating pressed pellets at 1100 °C for 5 d, cooling to 650 °C over 1 d, and holding there for 36 h, followed by quenching in cold water; (iii) heating pressed pellets at 1000 °C for 6 d, followed by cooling to room temperature over 24 h.

The ground products were analyzed by powder X-ray diffraction on a Rigaku Ultima IV diffractometer equipped with a D/teX Ultra detector and a Co K α radiation source operated at 38 kV and 38 mA. The compositions of any crystals extracted from the products were determined by energy-dispersive X-ray (EDX) analysis on a Zeiss Sigma 300 VP field-emission scanning electron microscope.

■ RESULTS AND DISCUSSION

Machine-Learning Model. To work toward the eventual goals of finding nonstoichiometric compounds between the ideal half-Heusler (ABC) and full-Heusler (AB₂C) structures, we first developed a machine-learning model to identify promising candidates ABC that are likely to adopt half-Heusler structures. Similar to many other classification problems in materials science, the desired half-Heusler candidates form only a small proportion of known ternary equiatomic compounds, and it is of interest to apply techniques in machine learning that address this class imbalance in the data set.⁴⁶

Machine-learning models were trained on a data set of 2818 ternary compounds extracted from Pearson's Crystal Data having an exact equiatomic composition ABC ("daltonides") and those that deviate from the ideal composition by up to 20% ("berthollides"). The data were classified into compounds that have half-Heusler structures (180) and those that do not (2638). The data were sorted in a similar way as described previously for determining site occupancies in half-Heusler structures (e.g., CBA to ABC) to reflect the most probable site occupancies, because the way that descriptors are defined is not order-invariant. 42 Descriptors were derived from elemental properties such as radii and electronegativities (Table S1 in the Supporting Information), which were combined through various arithmetic operations (Table S2 in the Supporting Information) and are assumed to be potential factors that control structure, similar to the empirical rules previously developed for half-Heusler structures. Including compounds having nonstoichiometric compositions, with their features weighted according to elemental content, helps to increase the data set to improve the machine-learning model; however, for the purpose of making predictions of new candidates, we restrict ourselves to stoichiometric compounds.

An ensemble approach combined with SMOTE was used to overcome the reliance on a single model, to cover chemical space more broadly, and to rectify the imbalance of data. The idea is to avoid misclassifications that could occur by overfitting in an individual model and to improve prediction probabilities, on the premise that multiple models can describe complementary areas of chemical space more effectively and that the majority decision is better than an individual one. For example, if one model assigns a probability of 90% that a candidate compound ABC has a half-Heusler structure, but two other models assign lower probabilities of 25%, the average probability becomes 47%, which would swing the decision about the prediction.

Table 1. Comparison of Model Performance

	training set		validation set			
model	sensitivity	specificity	accuracy	sensitivity	specificity	accuracy
before CR-FS/GA (ensemble)	0.857	0.937	0.969	0.733	0.971	0.964
after CR-FS (best individual)	0.800	0.996	0.922	0.650	0.985	0.817
after CR-FS/GA (ensemble)	0.900	0.989	0.978	0.867	0.983	0.975
after SMOTE (SVM CR-FS)	0.916	0.992	0.987	0.833	0.983	0.973
after SMOTE (KNN CR-FS)	0.733	0.977	0.961	0.666	0.981	0.961
after SMOTE (SVM GA)	0.833	0.993	0.983	0.733	0.985	0.969
after SMOTE (PLSDA GA)	0.933	0.959	0.957	0.883	0.957	0.953
after SMOTE (KNN GA)	0.525	0.990	0.961	0.666	0.994	0.973
after SMOTE (ensemble)	0.933	0.987	0.983	0.883	0.982	0.976

^aThe performance is evaluated for compounds having half-Heusler (HH) structures.

The results indicate that the ensemble approach is generally better than the use of a single model (Table 1), with an improved performance in the validation set. The machinelearning model was also improved by applying a feature selection (to avoid overfitting data) and SMOTE (to provide the model with more minority samples from which to learn), as shown by the increased sensitivity and accuracy. By applying two different feature selection methods, the number of models was increased from 3 to 6, and the number of features was reduced from 1155 to 225 (using GA) or 230 (using CR-FS). The number of synthetic samples introduced by SMOTE to the training sets is 52 (using GA) or 625 (using CR-FS), the large difference being attributed to how well these procedures cluster classes into homogeneous neighborhoods. Because we are interested in predicting new compounds with half-Heusler structures, the sensitivity (rate of true positives) is an especially important metric: the ensemble method applied together with SMOTE outperforms the best single-model method (SMOTE SVM CR-FS) by 6% in this regard.

In a previous assessment of first-principles versus machinelearning methods to discovery of half-Heusler compounds, Legrain et al. also developed a machine-learning model using a random forest algorithm (with 1000 trees).³⁹ A key difference is that Legrain's model was trained on ternary half-Heusler compounds with the ideal composition (1:1:1), whereas our model allowed deviations from the ideal composition by up to 20%. Legrain's model had a precision of 0.90, a sensitivity of 0.52, and a Matthew's correlation coefficient (MCC) of 0.68; in comparison, our model had a precision of 0.77, a sensitivity of 0.88, and an MCC of 0.82. Our model performs better in terms of balanced statistical measures and significantly fewer false negatives (higher MCC and sensitivity), but suffers in terms of more false positives (lower precision). In other words, our model is a bit overzealous in predicting compounds with new half-Heusler structures but overall exhibits better performance. Candidates having probabilities exceeding 90% of exhibiting half-Heusler structures are listed in Table S3 in the Supporting Information, and the top-ranked candidates are listed in Table 2. Among these, seven candidates (BiPrPt, BiSmPt, BiLuAu, BiYbNi, NbSbPt, MgBiPt, and ZrBiPt) overlap with predictions made by Legrain et al. with a milder threshold (>50% probability) of exhibiting half-Heusler structures.³⁹ Conversely, LaNiBi was predicted by Carrete et al. to be unstable in the half-Heusler structure,³⁴ in disagreement with the Open Quantum Materials Database.⁵¹

Half-Heusler Compounds with Full-Heusler Counterparts. For reasons as described in the introduction, it would be particularly interesting to discover new half-Heusler

Table 2. Top 25 Candidates of Adopting Half-Heusler Structures

sample	probability	sample	probability
BiLaNi	0.991	HfBiAu	0.953
PdCdBi	0.990	BiCeAu	0.952
BiLaAu	0.984	BiTbZn	0.951
BiLuAu	0.980	BiLaPb	0.951
SbTaNi	0.979	NiCdBi	0.949
BiPrPt	0.978	MgBiPt	0.947
BiLuHg	0.978	PdCdPb	0.946
BiLaHg	0.975	ZnPdBi	0.945
BiDyPd	0.972	ZnAgBi	0.944
BiLaZn	0.970	CdPtBi	0.944
BiCeHg	0.964	ZnRhBi	0.943
BiYbNi	0.964	ZnPdPb	0.942
BiSmPt	0.959		

compounds that have full-Heusler counterparts in hopes of forming a solid solution as a means of controlling physical properties. Currently, only 27 of these cases have been reported, of the hundreds of half-Heusler structures known (Table 3). The suspicion is that this should be a much more

Table 3. Known Half-Heusler Compounds having Full-Heusler Counterparts

AlGeLi	GaMnPt	MnPdSb
BiLiMg	GaMnRu	MnPtSn
CoNbSn	HfNiSn	NiSbTi
CoSbTi	HfPdSn	NiSnTi
CoSnTa	LiMgSb	NiSnU
CoSnTi	LiPZn	NiSnZr
CuMnSb	MgNiSb	PdSbY
FeSnTi	MgPdSb	PdSnZr
GaIrMn	MnNiSb	PtScSn

common phenomenon, but the chemical space has not yet been extensively explored, and the structures of intermediate members may not be straightforward to determine. Inspecting the frequency of occurrence of elements in reported half-Heusler compounds reveals that more than half of the cases involve group 10 elements (Ni, Pd, Pt); in fact, \sim 40% of all half-Heusler compounds contain Ni (Figure S1a in the Supporting Information). The 18-electron rule has often been proposed as a condition for the formation of half-Heusler compounds. For example, this rule can be satisfied by combining Ni (10 e $^-$) with rare-earth metals (3 e $^-$) and a

Table 4. Candidates with Probabilities of Greater than 50% of Adopting Half-Heusler Structures having Existing Full-Heusler Counterparts

sample	probability	sample	probability	sample	probability
MnRhPb	0.935	PdPbLi	0.748	MnSnCo	0.652
SbUPd	0.922	TiBiLi	0.741	MnRhAl	0.636
MnSnPd	0.918	LiZnSn	0.738	LiAlPd	0.631
MnRhSn	0.895	LiMgSi	0.728	LiMgIn	0.627
MnPdIn	0.885	YBiPd	0.727	VSnCo	0.625
MnPdSn	0.883	MgPdIn	0.723	TiPbLi	0.623
MnSnNi	0.879	TiSnLi	0.720	SnPtLi	0.613
LiCdGe	0.869	MnRuSb	0.719	LiMgTl	0.606
MnSnCu	0.866	LiCdSn	0.711	SnIrLi	0.593
MgSnNi	0.863	LiGeNi	0.707	LiMgCd	0.586
ZrSbPt	0.861	MnAuAl	0.703	LiNiSi	0.583
LiMgGe	0.826	NiZnSn	0.702	LiGaRh	0.563
LiMgPb	0.795	MnRuSn	0.698	VSnRh	0.556
LiSbSn	0.785	SbPtZr	0.698	VPbLi	0.553
VSnNi	0.779	SnHfCo	0.695	TiSnIr	0.546
LiHgGe	0.778	VSnFe	0.692	MgInAg	0.538
LiSbCo	0.777	TiSnRu	0.676	LiSbNa	0.535
TiSnPd	0.768	LiGeCo	0.675	LiGeRh	0.533
LiMgSn	0.758	MgInNi	0.675	MgPdGa	0.525
MnPdAl	0.756	LiSbCu	0.664	CrSnRu	0.518
LiMgGa	0.751	LiNiSn	0.659	LiSnRh	0.515
NbSnNi	0.749	LiPdGe	0.652		

group 15 element such as Sb (5 e⁻), which is the most frequently encountered element occurring in 46% of all half-Heusler compounds. Another common combination of elements is Ni (10 e⁻), group 4 elements (4 e⁻), and Sn (4 e⁻), which also satisfies the 18-electron rule. However, an objective appraisal shows that the 18-electron rule is violated for nearly half of all reported half-Heusler compounds, raising doubts about the universal validity of this rule. In comparison to these known compounds, the machine-learning model suggests that many candidates predicted to adopt half-Heusler structures contain either Sb or Bi (Figure S1b in the Supporting Information).

From the machine-learning model developed above, a subset of 58 candidates having greater than 50% probabilities of adopting half-Heusler structures not previously reported in Pearson's Crystal Data were suggested that have an existing full-Heusler counterpart (Table 4). The crucial next step is to validate some of these predictions through experiment. Initially, a few candidates were selected with varying probabilities of adopting half-Heusler structures: MnNiSn (88%), MnRuSb (72^{-}), and VRhSn (56%). Although it has a lower probability of forming a half-Heusler structure, VRhSn was an interesting candidate to examine, because VRh₂Sn is known to exist as two polymorphs (room-temperature tetragonal structure and high-temperature full-Heusler structure).⁵² Attempts were made to prepare MnNiSn, MnRuSb, and VRhSn by reaction of the elements in equimolar ratios through arc-melting followed by annealing at 800 °C. Small crystals extracted from the samples were examined by scanning electron microscopy, and EDX analysis indicated compositions of $Mn_{1.0}Ni_{1.5}Sn_{1.0}$, $Mn_{1.0}Ru_{1.8}Sb_{1.0}$, and $V_{1.5}Rh_{1.5}Sn_{1.0}$. In retrospect, these nonequiatomic compositions are understandable because of losses occurring during arc-melting (Mn and Sb are easily volatilized, and Sn has a low melting point). Although the desired half-Heusler compounds having strictly equiatomic compositions were not obtained, the nonstoichiometric formulas suggest the occurrence of solid solutions subject to vacancy defects (MnNi_{2-x}Sn, MnRu_{2-x}Sb) or substitutional disorder ($(V_{1-x}Rh_x)_3Sn$).

This outcome illustrates the important point that theoretical predictions for the structure of a compound (let alone its existence), whether made by first-principles or machinelearning methods, should not be confused with the synthesizability of a compound, which is a different matter. 53 The experimental chemist has practical considerations to make and different challenges to overcome in synthesis and characterization. Nevertheless, the predictions can help guide the choice of ternary systems to examine. Subsequently, several of the top-ranked candidates together with the previous three (MnRhPb, MnPdSn, MnRhSn, MnPdIn, MnNiSn, MnRuSb, VRhSn) were targeted for preparation by a similar arc-melting and annealing procedure as before, except that an excess of the volatile components (e.g., Mn, Sb) was added to compensate for losses during arc-melting. Except for the MnRhPb sample, which was found to contain a mixture of binary phases, the powder XRD patterns reveal that the desired ternary compounds were formed (Figure 3). Note that most samples contain other secondary phases, because the syntheses have not yet been optimized (but the MnPdIn sample appears to be relatively pure). EDX analyses indicated average compositions $of \quad Mn_{0.36}Pd_{0.38}Sn_{0.27}, \quad Mn_{0.36}Rh_{0.33}Sn_{0.31}, \quad Mn_{0.29}Pd_{0.33}In_{0.38},$ $Mn_{0.34}Ni_{0.35}Sn_{0.31}$, $Mn_{0.28}Ru_{0.39}Sb_{0.34}$, and $V_{0.32}Rh_{0.33}Sn_{0.35}$, in reasonable agreement with expectations. The cell parameters for these half-Heusler compounds are generally smaller than those reported for the full-Heusler counterparts (Table S4 in the Supporting Information). MnPdIn and VRhSn appear to violate this trend, having cell parameters identical to or even slightly greater than the full-Heusler counterparts, although it should be noted that, in many other instances of pairs of halfand full-Heusler structures, the differences in cell parameters can be nearly negligible. In these cases, it would be worthwhile to reinvestigate the previously reported full-Heusler structures.

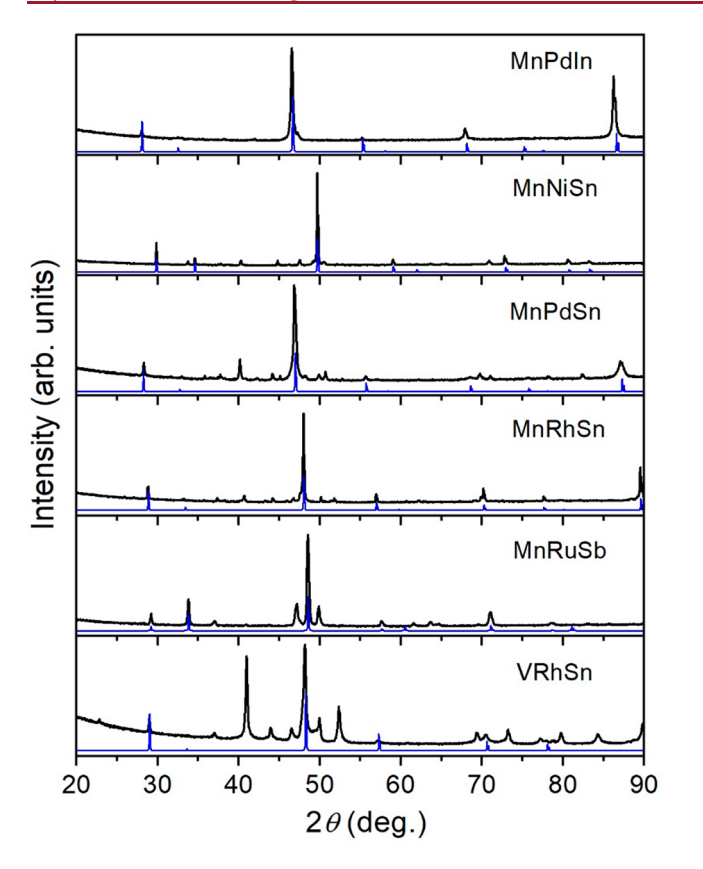


Figure 3. Powder XRD patterns (obtained using Co $K\alpha$ radiation) of samples prepared from arc-melting and annealing. Simulated patterns for half-Heusler structures are shown in blue.

Another explanation could be that some degree of disorder may be taking place if the compositions are slightly offstoichiometry. This is not a trivial problem to resolve at this stage because of the multiple ways that disorder can occur. An analysis of all reported half-Heusler structures, including those exhibiting disorder, shows which elements are likely to mix within each of the three crystallographic sites (Figure 4). Of course, it is not surprising that chemically similar elements are the ones that disorder with each other; for example, in MnNi_{0.5}Pt_{0.5}Sb, the 4c site contains a mixture of Ni and Pt atoms. 34 However, disorder can also occur between apparently dissimilar elements; for example, in Mn_{1.5}Ni_{0.75}Sb_{0.75}, the 4a site contains a mixture of Mn and Sb atoms, and the 4b site contains a mixture of Mn and Ni atoms.⁵⁵ At the extreme, all three sites are subject to disorder, as seen in $Hf_{0.5}Zr_{0.5}Co_{0.5}Rh_{0.5}Sn_{0.01}Sb_{0.99}$. Finally, varying experimental conditions may lead to different types and degrees of disorder.⁵⁷ Auxiliary machine-learning tools to assist in site assignments may prove helpful.58

In addition to confirming positive predictions from the machine-learning model, testing negative predictions is important to evaluate the degree to which false negative errors arise. An equal number of "unlikely" candidates (CrGaSn, CrMoNi, CuRuNb, MoHfNi, NiAgNb, VHfAg, ZrRuNb) were identified that have low probabilities (<50%) of adopting half-Heusler structures and that contain at least one component in common with the high-probability candidates characterized above. Reactions targeting these compounds were attempted under similar conditions (arc-melting; direct reactions at 1000 or 1100 °C) as before. The powder XRD patterns of the

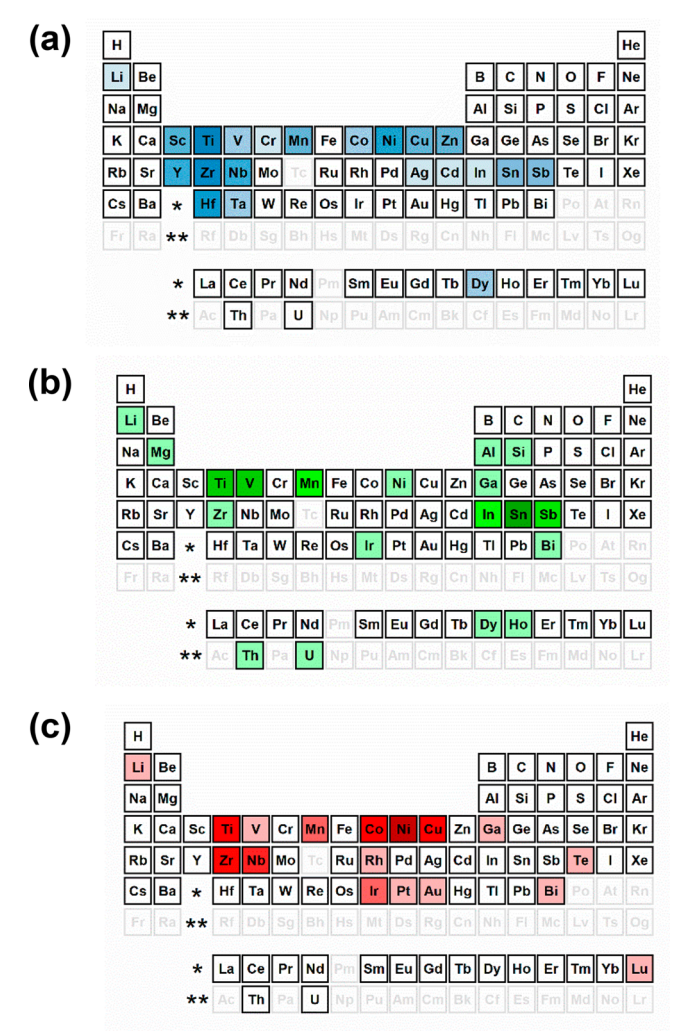


Figure 4. Likelihood of elements to undergo mixing within sites (4a, 4b, 4c) in half-Heusler (MgAgAs-type) structures that exhibit substitutional disorder. The intensity of the color is proportional to the frequency that this mixing has occurred within 83 unique cases (with complete structure determination) as reported in Pearson's Crystal Data.

samples do not match at all with the simulated patterns expected for half-Heusler structures (Figure S2 in the Supporting Information). In other words, the negative predictions of the machine-learning model are correct for seven of seven samples, with no false negative results.

CONCLUSIONS

The illusion that Heusler compounds are straightforward to understand is shattered when disorder is introduced. In fact, the analysis presented here highlights the challenges of classifying structures into distinct types in the first place, let alone predicting them by either first-principles or machine-learning methods. The machine-learning model developed here includes nonstoichiometric compounds as part of the training set; it made use of techniques of oversampling (SMOTE) to correct for unbalanced data sets typical of materials chemistry problems, and soft voting over an ensemble of algorithms to improve performance. On the basis of this model, predictions were made of candidate compounds that are likely to adopt half-Heusler structures that have existing full-Heusler counterparts. Of seven arbitrarily

selected candidates, six were successfully synthesized and were confirmed experimentally to be half-Heusler compounds. The next steps are to further characterize these compounds, in particular, to determine the site occupancies and to ascertain the nature of disorder, if any, within their structures, and to prepare members of a solid solution between a pair of related half- and full-Heusler compounds.

ASSOCIATED CONTENT

Supporting Information

The Supporting Information is available free of charge at https://pubs.acs.org/doi/10.1021/acs.cgd.0c00646.

Elemental properties and arithmetic operations applied to them, machine-learning probabilities, cell parameters, frequency of occurrence of elements in half-Heusler structures, and additional powder XRD patterns (PDF)

AUTHOR INFORMATION

Corresponding Author

Arthur Mar — Department of Chemistry, University of Alberta, Edmonton, Alberta T6G 2G2, Canada; o orcid.org/0000-0003-0474-5918; Email: amar@ualberta.ca

Authors

Alexander S. Gzyl – Department of Chemistry, University of Alberta, Edmonton, Alberta T6G 2G2, Canada

Anton O. Oliynyk — Department of Chemistry, University of Alberta, Edmonton, Alberta T6G 2G2, Canada; Department of Chemistry and Biochemistry, Manhattan College, Riverdale, New York 10741, United States; orcid.org/0000-0003-0732-7340

Complete contact information is available at: https://pubs.acs.org/10.1021/acs.cgd.0c00646

Notes

The authors declare no competing financial interest.

ACKNOWLEDGMENTS

This work was supported by the Canada First Research Excellence Fund (CFREF, through the Future Energy Systems Research Institute at the University of Alberta, Project No. T12-P01), the Natural Sciences and Engineering Research Council of Canada (NSERC, through Discovery Grant No. RGPIN-2018-04294), and the NSERC Collaborative Research and Training Experience Program (CREATE, through the Alberta/Technical University of Munich International Graduate School).

REFERENCES

- (1) Graf, T.; Felser, C.; Parkin, S. S. P. Simple rules for the understanding of Heusler compounds. *Prog. Solid State Chem.* **2011**, 39, 1–50.
- (2) Felser, C., Hirohata, A., Eds. Heusler Alloys: Properties, Growth, Applications; Springer: Berlin, Germany, 2016.
- (3) Bos, J.-W. G.; Downie, R. A. Half-Heusler thermoelectrics: a complex class of materials. *J. Phys.: Condens. Matter* **2014**, *26*, 433201.
- (4) Zeier, W. G.; Schmitt, J.; Hautier, G.; Aydemir, U.; Gibbs, Z. M.; Felser, C.; Snyder, G. J. Engineering half-Heusler thermoelectric materials using Zintl chemistry. *Nat. Rev. Mater.* **2016**, *1*, 16032.
- (5) Poon, S. J. Half-Heusler compounds: promising materials for mid-to-high temperature thermoelectric conversion. *J. Phys. D: Appl. Phys.* **2019**, *52*, 493001.

- (6) Felser, C.; Wollmann, L.; Chadov, S.; Fecher, G. H.; Parkin, S. S. P. Basics and prospective of magnetic Heusler compounds. *APL Mater.* **2015**, *3*, 041518.
- (7) Palmstrøm, C. J. Heusler compounds and spintronics. *Prog. Cryst. Growth Charact. Mater.* **2016**, 62, 371–397.
- (8) Planes, A.; Mañosa, L.; Acet, M. Magnetocaloric effect and its relation to shape-memory properties in ferromagnetic Heusler alloys. *J. Phys.: Condens. Matter* **2009**, *21*, 233201.
- (9) Yan, B.; de Visser, A. Half-Heusler topological insulators. MRS Bull. 2014, 39, 859–866.
- (10) Manna, K.; Sun, Y.; Muechler, L.; Kübler, J.; Felser, C. Heusler, Weyl and Berry. Nat. Rev. Mater. 2018, 3, 244-256.
- (11) Acet, M.; Wassermann, E. F. Magnetic interactions in Ni-Mn-based magnetic shape-memory Heusler alloys. *Adv. Eng. Mater.* **2012**, *14*, 523–529.
- (12) Kojima, T.; Kameoka, S.; Tsai, A.-P. The emergence of Heusler alloy catalysts. Sci. Technol. Adv. Mater. 2019, 20, 445–455.
- (13) The term "Heusler compounds" could refer to the larger family of compounds encompassing several compositions or, more specifically, to the subset adopting the structure type of Cu₂MnAl, which was among the original compounds studied by Fritz Heusler a century ago. To avoid confusion, compounds adopting the Cu₂MnAl-type structure will be referred to explicitly as "full-Heusler compounds." Strukturbericht designations are also eschewed, because they are obsolete, opaque, and not recommended by IUPAC.
- (14) Felser, C.; Alijani, V.; Winterlik, J.; Chadov, S.; Nayak, A. K. Tetragonal Heusler compounds for spintronics. *IEEE Trans. Magn.* **2013**, *49*, 682–685.
- (15) Wu, M.; Han, Y.; Bouhemadou, A.; Cheng, Z.; Khenata, R.; Kuang, M.; Wang, X.; Yang, T.; Yuan, H.; Wang, X. Site preference and tetragonal distortion in palladium-rich Heusler alloys. *IUCrJ* **2019**, *6*, 218–225.
- (16) Villars, P.; Cenzual, K. Pearson's Crystal Data Crystal Structure Database for Inorganic Compounds, on DVD, rel. 2018/19; ASM International: Materials Park, OH, 2018.
- (17) Bacon, G. E.; Plant, J. S. Chemical ordering in Heusler alloys with the general formula A_2BC or ABC. J. Phys. F: Met. Phys. 1971, 1, 524–532.
- (18) Kouacou, M. A.; Koua, A. A.; Zoueu, J. T.; Konan, K.; Pierre, J. Onset of itinerant ferromagnetism associated with semiconductormetal transition in Ti_xNb_{11x}CoSn half Heusler solid solution compound. *Pramana* **2008**, *71*, 157–166.
- (19) Chauhan, N. S.; Gahtori, B.; Sivaiah, B.; Mahanti, S. D.; Dhar, A.; Bhattacharya, A. Modulating the lattice dynamics of n-type Heusler compounds via tuning Ni concentration. *Appl. Phys. Lett.* **2018**, *113*, 013902.
- (20) Nagasako, M.; Taguchi, Y.; Miyamoto, T.; Kanomata, T.; Ziebeck, K. R. A.; Kainuma, R. Order-disorder transition of vacancies from the full- to the half-Heusler structure in Ni_{2-x}MnSb alloys. *Intermetallics* **2015**, *61*, 38–41.
- (21) Levin, E. E.; Bocarsly, J. D.; Wyckoff, K. E.; Pollock, T. M.; Seshadri, R. Tuning the magnetocaloric response in half-Heusler/Heusler MnNi $_{1+x}$ Sb solid solutions. *Phys. Rev. Mater.* **2017**, *1*, 075003.
- (22) Makongo, J. P. A.; Misra, D. K.; Zhou, X.; Pant, A.; Shabetai, M. R.; Su, X.; Uher, C.; Stokes, K. L.; Poudeu, P. F. P. Simultaneous large enhancements in thermopower and electrical conductivity of bulk nanostructured half-Heusler alloys. *J. Am. Chem. Soc.* **2011**, *133*, 18843–18852.
- (23) Page, A.; Uher, C.; Poudeu, P. F.; Van der Ven, A. Phase separation of full-Heusler nanostructures in half-Heusler thermoelectrics and vibrational properties from first-principles calculations. *Phys. Rev. B: Condens. Matter Mater. Phys.* **2015**, 92, 174102.
- (24) Bhardwaj, A.; Chauhan, N. S.; Sancheti, B.; Pandey, G. N.; Senguttuvan, T. D.; Misra, D. K. Panoscopically optimized thermoelectric performance of a half-Heusler/full-Heusler based *in situ* bulk composite $Zr_{0.7}Hf_{0.3}Ni_{1+x}Sn$: an energy and time efficient way. *Phys. Chem. Chem. Phys.* **2015**, *17*, 30090–30101.

- (25) Kocevski, V.; Wolverton, C. Designing high-efficiency nanostructured two-phase Heusler thermoelectrics. *Chem. Mater.* **2017**, 29, 9386–9398.
- (26) Spataru, C. D.; He, Y.; Léonard, F. Atomistic study of an ideal metal/thermoelectric contact: The full-Heusler/half-Heusler interface. *APL Mater.* **2019**, *7*, 013202.
- (27) Müller, U. Symmetry Relationships between Crystal Structures; Oxford University Press: Oxford, UK, 2013.
- (28) Bende, D.; Grin, Y.; Wagner, F. R. Covalence and ionicity in MgAgAs-type compounds. *Chem. Eur. J.* **2014**, *20*, 9702–9708.
- (29) Faleev, S. V.; Ferrante, Y.; Jeong, J.; Samant, M. G.; Jones, B.; Parkin, S. S. P. Unified explanation of chemical ordering, the Slater-Pauling rule, and half-metallicity in full Heusler compounds. *Phys. Rev. B: Condens. Matter Mater. Phys.* **2017**, *95*, 045140.
- (30) Wang, X.; Cheng, Z.; Yuan, H.; Khenata, R. L2₁ and XA ordering competition in titanium-based full-Heusler alloys. *J. Mater. Chem. C* **2017**, *S*, 11559–11564.
- (31) White, M. A.; Medina-Gonzalez, A. M.; Vela, J. Soft chemistry, coloring and polytypism in filled tetrahedral semiconductors: Toward enhanced thermoelectric and battery materials. *Chem. Eur. J.* **2018**, 24, 3650–3658.
- (32) Anand, S.; Xia, K.; Hegde, V. I.; Aydemir, U.; Kocevski, V.; Zhu, T.; Wolverton, C.; Snyder, G. J. A valence balanced rule for discovery of 18-electron half-Heuslers with defects. *Energy Environ. Sci.* **2018**, *11*, 1480–1488.
- (33) Zhang, X.; Yu, L.; Zakutayev, A.; Zunger, A. Sorting stable versus unstable hypothetical compounds: The case of multi-functional ABX half-Heusler filled tetrahedral structures. *Adv. Funct. Mater.* **2012**, 22, 1425–1435.
- (34) Carrete, J.; Li, W.; Mingo, N.; Wang, S.; Curtarolo, S. Finding unprecedently low-thermal-conductivity half-Heusler semiconductors via high-throughput materials modeling. *Phys. Rev. X* **2014**, *4*, 011019.
- (35) Ma, J.; Hegde, V. I.; Munira, K.; Xie, Y.; Keshavarz, S.; Mildebrath, D. T.; Wolverton, C.; Ghosh, A. W.; Butler, W. H. Computational investigation of half-Heusler compounds for spintronics applications. *Phys. Rev. B: Condens. Matter Mater. Phys.* **2017**, 95, 024411.
- (36) He, J.; Naghavi, S. S.; Hegde, V. I.; Amsler, M.; Wolverton, C. Designing and discovering a new family of semiconducting quaternary Heusler compounds based on the 18-electron rule. *Chem. Mater.* **2018**, *30*, 4978–4985.
- (37) Kim, K.; Ward, L.; He, J.; Krishna, A.; Agrawal, A.; Wolverton, C. Machine-learning-accelerated high-throughput materials screening: Discovery of novel quaternary Heusler compounds. *Phys. Rev. Mater.* **2018**, *2*, 123801.
- (38) Gao, Q.; Opahle, I.; Zhang, H. High-throughput screening for spin-gapless semiconductors in quaternary Heusler compounds. *Phys. Rev. Mater.* **2019**, *3*, 024410.
- (39) Legrain, F.; Carrete, J.; van Roekeghem, A.; Madsen, G. K. H.; Mingo, N. Materials screening for the discovery of new half-Heuslers: Machine learning versus ab initio methods. *J. Phys. Chem. B* **2018**, 122, 625–632.
- (40) "Heads, I win. Tails, you forget we had a bet." Tetlock, P. E.; Gardner, D. In Superforecasting: the art of science and prediction; Penguin Random House: New York, 2015.
- (41) Oliynyk, A. O.; Antono, E.; Sparks, T. D.; Ghadbeigi, L.; Gaultois, M. W.; Meredig, B.; Mar, A. High-throughput machine-learning-driven synthesis of full-Heusler compounds. *Chem. Mater.* **2016**, 28, 7324–7331.
- (42) Gzyl, A. S.; Oliynyk, A. O.; Adutwum, L. A.; Mar, A. Solving the coloring problem in half-Heusler structures: Machine-learning predictions and experimental validation. *Inorg. Chem.* **2019**, *58*, 9280–9289.
- (43) Oliynyk, A. O.; Mar, A. Discovery of intermetallic compounds from traditional to machine-learning approaches. *Acc. Chem. Res.* **2018**, *51*, 59–68.
- (44) Chawla, N. V.; Bowyer, K. V.; Hall, L. O.; Kegelmeyer, W. P. SMOTE: Synthetic minority over-sampling technique. *J. Artif. Intell. Res.* **2002**, *16*, 321–357.

- (45) Meredig, B.; Antono, E.; Church, C.; Hutchinson, M.; Ling, J.; Paradiso, S.; Blaiszik, B.; Foster, I.; Gibbons, B.; Hattrick-Simpers, J.; Mehta, A.; Ward, L. Can machine learning identify the next high-tempreature superconductor? Examining extrapolation performance for materials discovery. *Mol. Syst. Des. Eng.* **2018**, *3*, 819–825.
- (46) Kailkhura, B.; Gallagher, B.; Kim, S.; Hiszpanski, A.; Han, T. Y.-J. Reliable and explainable machine-learning methods for accelerated material discovery. *npj. Comput. Matter* **2019**, *5*, 108.
- (47) PLS_Toolbox, ver. 8.0.1; Eigenvector Research Inc.: Wenatchee, WA, 2018.
- (48) MATLAB Statistics and Machine Learning Toolbox, rel. 2018a; The Mathworks Inc.: Natick, MA, 2018.
- (49) Sinkov, N. A.; Harynuk, J. J. Cluster resolution: A metric for automated, objective and optimized feature selection in chemometric modeling. *Talanta* **2011**, *83*, 1079–1087.
- (50) Jennings, P. C.; Lysgaard, S.; Hummelshøj, J. S.; Vegge, T.; Bligaard, T. Genetic algorithms for computational materials discovery accelerated by machine learning. *npj Comput. Mater.* **2019**, *5*, 46.
- (51) Kirklin, S.; Saal, J. E.; Meredig, B.; Thompson, A.; Doak, J. W.; Aykol, M.; Rühl, S.; Wolverton, C. The Open Quantum Materials Database (OQMD): assessing the accuracy of DFT formation energies. *npj Comput. Mater.* **2015**, *1*, 15010.
- (52) Suits, J. C. Structural instability in new magnetic Heusler compounds. *Solid State Commun.* **1976**, *18*, 423–425.
- (53) Aykol, M.; Hegde, V. I.; Hung, L.; Suram, S.; Herring, P.; Wolverton, C.; Hummelshøj, J. S. Network analysis of synthesizable materials discovery. *Nat. Commun.* **2019**, *10*, 2018.
- (54) van Engelen, P. P. J.; de Mooij, D. B.; Wijngaard, J. H.; Buschow, K. H. J. Magneto-optical and magnetic properties of some solid solutions of C1_b-Heusler compounds. *J. Magn. Magn. Mater.* **1994**, *130*, 247–254.
- (55) Pacurariu, R.; Rednic, V.; Coldea, M.; Benea, D.; Pop, V.; Isnard, O.; Neumann, M. Effects of substitution of Ni by Sb in MnNi. *Phys. Status Solidi B* **2009**, 246, 50–55.
- (56) Maji, P.; Takas, N. J.; Misra, D. K.; Gabrisch, H.; Stokes, K.; Poudeu, P. F. P. Effects of Rh on the thermoelectric performance of the *p*-type Zr_{0.5}Hf_{0.5}Co_{11x}Rh_xSb_{0.99}Sn_{0.01} half-Heusler alloys. *J. Solid State Chem.* **2010**, *183*, 1120–1126.
- (57) Zhang, H. G.; Zhang, C. Z.; Zhu, W.; Liu, E. K.; Wang, W. H.; Zhang, H. W.; Cheng, J. L.; Luo, H. Z.; Wu, G. H. Significant disorder-induced enhancement of the magnetization of Fe₂CrGa by ball milling. *J. Appl. Phys.* **2013**, *114*, 013903.
- (58) Viswanathan, G.; Oliynyk, A. O.; Antono, E.; Ling, J.; Meredig, B.; Brgoch, J. Single-crystal automated refinement (SCAR): A data-driven method for determining inorganic structures. *Inorg. Chem.* **2019**, *58*, 9004–9015.